TOPICAL REVIEW • OPEN ACCESS

The 'skin effect' of subsurface damage distribution in materials subjected to high-speed machining

Topical Review

The 'skin effect' of subsurface damage distribution in materials subjected to high-speed machining

Bi Zhang[1,2] **and Jingfei Yin**[3]

[1] The Southern University of Science and Technology, Shenzhen, People's Republic of China
[2] The University of Connecticut, Storrs, CT, United States of America
[3] Dalian University of Technology, Dalian, People's Republic of China

E-mail: Zhangb@SUSTech.edu.cn, bi.zhang@uconn.edu and 2296302449@qq.com

CrossMark

Abstract

This paper proposes the 'skin effect' of the machining-induced damage at high strain rates. The paper first reviews the published research work on machining-induced damage and then identifies the governing factors that dominate damage formation mechanisms. Among many influential factors, such as stress–strain field, temperature field, material responses to loading and loading rate, and crack initiation and propagation, strain rate is recognized as a dominant factor that can directly lead to the 'skin effect' of material damage in a loading process. The paper elucidates that material deformation at high strain rates ($>10^3 \, \text{s}^{-1}$) leads to the embrittlement, which in turn contributes to the 'skin effect' of subsurface damage. The paper discusses the 'skin effect' based on the principles of dislocation kinetics and crack initiation and propagation. It provides guidance to predicting the material deformation and damage at a high strain-rate for applications ranging from the armor protection, quarrying, petroleum drilling, and high-speed machining of engineering materials (e.g. ceramics and SiC reinforced aluminum alloys).

Keywords: skin effect, strain rate, dislocation, embrittlement, damage

(Some figures may appear in colour only in the online journal)

1. Introduction

The term 'skin effect' has been used to describe distribution of the alternating current in a conductor that electric current mainly flows in the 'skin' layer of the conductor. The current density is the highest at the surface layer of the conductor and quickly decreases in the inner layers. The 'skin effect' is further strengthened at a higher frequency of the alternating current. Similarly, the authors have found that the 'skin effect' of subsurface damage (SSD) distribution also exists in

material deformations. The 'skin effect' of SSD distribution can be enhanced at a higher strain rate in a loading process.

Generally, an increased strain-rate results in embrittlement of the material subjected to loading, which in turn leads to the 'skin effect'. For example, in armor applications, the brittleness of the material greatly affects the ballistic performance of an armor. Ceramics generally have better resistance to the ballistic impact than metallic materials [1, 2]. Another example is the high-speed machining (HSM) of engineering materials, such as ceramics and SiC reinforced aluminum alloys. High speeds of machining could embrittle the workpiece material and suppress SSD depth because of the 'skin effect'.

We are living in a world that needs support from various materials. How these materials may serve our purposes has been a subject of study. Some materials are harder and more
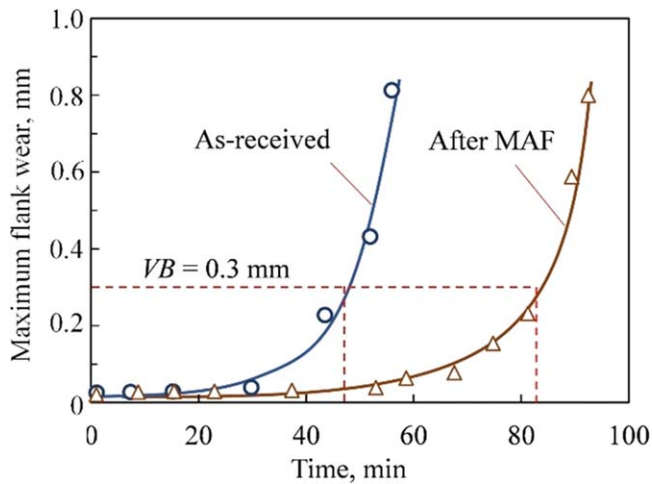
Figure 1. Maximum flank wear of the different tool inserts versus machining time (cutting speed: 100 m min^{-1}, feed: 75 μm/rev, depth of cut: 1.0 mm, coolant: 5% vol. trim solution). Reprinted from [23], Copyright (2012), with permission from Elsevier.

brittle (e.g. ceramics, semiconductors, cast irons) than others (e.g. most metals). It is necessary to shape the materials into various products with the help of modern manufacturing technologies, such as machining, laser beam cutting, forming, forging and welding. On the other hand, we want the products to perform the functions as we desire. These functions may include strength and toughness, fatigue strength (e.g. aircraft engines and bridges), wear resistance (e.g. bearings and cutting tools), etc. To achieve the respective functions, the right materials must be chosen for the appropriate applications. Titanium, Inconel, and aluminum alloys, for example, are normally used in the aerospace applications [3, 4]. Crystalline silicon is a typical substrate material for the semiconductor [5–7] and photovoltaic industries [8, 9]. Sapphire is used as the substrate material for LEDs [10–12]. Ceramics have been used in the high-precision bearings and cutting tools [13, 14]. Glasses are indispensable materials for optics and light transmission [15]. However, the above-mentioned materials can easily be induced with SSD when they are subjected to machining.

In machining of titanium, Inconel and aluminum alloys, work hardening and tool wear are notable, resulting in a metamorphic layer on the machined surface [16–19]. Generally, the metamorphic layer degrades the service performance of a part because of the different mechanical properties from the bulk material, such as hardness, toughness, and plasticity [20, 21]. On the other hand, materials, such as SiC, sapphire, and silicon, are hard and brittle, and can easily be introduced with SSD during a machining process [7, 15, 22], which is detrimental to the performance and lifetime of a part.

As shown in figure 1, an as-received cutting tool insert offered a lifetime of approximately 49 min. However, when another insert of the same batch from the same manufacturer was finished by the magnetic abrasive finishing (MAF) technique, its lifetime was 86 min, almost doubling the lifetime of the as-received version. Why should this happen? What is the function of MAF on the lifetime of the insert?
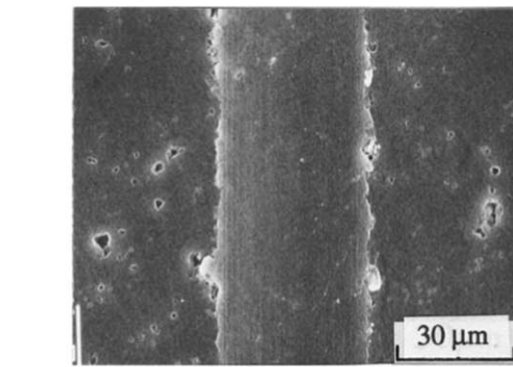
(a) Top view
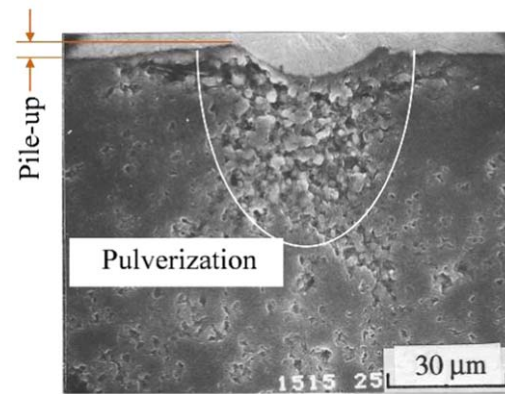
(b) Cross-sectional view

Figure 2. SEM images of (a) top view and (b) cross-sectional view of a smooth groove generated by grinding in an alumina sample. [24] (1988) © Chapman and Hall Ltd. With permission of Springer.

To answer these questions, an early work conducted by Zhang *et al* [24, 25] should be referred to. In their work, Zhang *et al* produced a smooth groove in a hot-pressed alumina sample in the single-point grinding process at a speed of 1800 m min^{-1}. Figure 2 shows the images of the groove taken from the top and cross-sectional views by a scanning electron microscope (SEM). Figure 2(a) presents the top view of the groove with a smooth surface. Although the groove did not show any observable damage (e.g. cracking, chipping), its subsurface was severely damaged with a layer of pulverization, as shown in figure 2(b). Moreover, the cross-sectional view reveals that material pile-up occurred to the two sides of the groove. The pile-up was clearly because of the side flow of the pulverized material. Therefore, pile-up does not have to be plastic deformation in the machining of the hard and brittle materials.

Based on the understanding of figure 2, it is suggested that the cutting edge of the as-received insert in figure 1 should have been left with the grinding-induced SSD which is responsible for the compromised tool life. Upon the removal of SSD by the MAF technique, tool life was largely extended, as depicted in figure 1. Therefore, the removal of the machining-induced damage is beneficial to the improvement of the performance and lifetime of a cutting tool.

Over the years, continuous efforts have been made in machining of hard and brittle materials. Bifano *et al* [26] were

the first to propose the 'ductile-regime' machining technique for brittle materials to achieve high-quality grinding. Although 'ductile-regime' machining has received much attention, it is still controversial as it lacks both theoretical and experimental support. This technique is mainly concerned with surface finish with no consideration of SSD of a machined workpiece. It has not solved the machining problems of the hard and brittle materials.

In order to solve these problems, Zhang *et al* [25] used a different approach. They not only investigated the surface but also the subsurface characteristics of a machined workpiece. They were the first to report the material pulverization mechanism together with the other forms of machining-induced SSD in ceramics [24, 25, 27–30]. Their findings have been applied in industry for high efficiency and low damage machining of ceramic materials.

Ultrasonically-assisted machining (UAM) has successfully been used in reducing machining force and improving surface integrity for the hard and brittle materials [31–35]. In fact, UAM helps suppress machining-induced damage, enhance the critical depth of cut [31], reduce machining forces [32, 36], and alter material properties [37]. UAM has a great potential for machining of the hard and brittle materials, however, there are still critical issues to be resolved. The issues include how UAM suppresses the machining-induced damage and improves workpiece surface integrity.

HSM has attracted much attention because of its improvement in machining efficiency, reduction in tool wear, and suppression in workpiece damage as compared to the conventional machining [38–40]. HSM can be applied to many different materials with no specific requirements on the workpiece properties. Most of all, HSM leads to a high strain rate which results in the so-called 'skin effect', namely, the machining-induced SSD tends to distribute in the superficial layer of a workpiece machined at a high strain rate [41–45]. Therefore, HSM presents a huge potential in high-efficiency machining of the above-mentioned materials. However, the underlying mechanisms of the 'skin effect' of SSD distribution remain unrevealed and need investigations.

This paper is to explore the mechanisms of the 'skin effect' of SSD at high strain rates and its application to HSM. Among the differences between HSM and the low-speed machining, the strain rate is the primary factor. This paper presents the 'skin effect' of SSD distribution at high strain rates ($>10^3\,\text{s}^{-1}$) with section 2 dealing with the 'skin effect' of machining-induced damage. Section 3 discusses the underlying mechanisms of the 'skin effect' at high strain rates; section 4 discusses the 'skin effect' in terms of dislocation and energy theories; section 5 concludes the paper and presents an outlook.

2. 'Skin-effect' of damage at high strain rates

In machining, the plastic strain rate $d\varepsilon/dt$ is regarded as a function of rake angle γ of a cutting tool, shear angle φ, cutting speed V, and the elemental chip thickness Δy, as

presented in equation (1) [46, 47],

$$\frac{d\varepsilon}{dt} = \frac{V \cos \gamma}{\Delta y \cos (\varphi - \gamma)}, \tag{1}$$

where the elemental chip thickness is related to the depth of cut. However, equation (1) cannot be used to calculate the strain rate in the machining of hard and brittle materials because these materials do not normally show notable plastic deformation before fracturing. Wang *et al* proposed a simple formula for calculating strain rate, shown as equation (2) [48],

$$\frac{d\varepsilon}{dt} = \frac{V}{a_c}, \tag{2}$$

where a_c represents depth of cut. Equation (2) describes strain rate in the region of a material compressed by a cutting tool. In this study, equation (2) is adopted to calculate strain rate based on the previous studies. As shown in figure 3, the SSD depth in the hard and brittle materials decreases with an increase in strain rate of machining, which well depicts the 'skin effect' of damage formation in terms of strain rate. The best fitting line in figure 3 shows that the SSD depth is mathematically proportional to the negative exponent of strain rate, as presented in equation (3),

$$\delta = k \cdot \left(\frac{d\varepsilon}{dt} \right)^{-0.34}, \tag{3}$$

where k is a constant ($k = 1531$ in figure 3).

In addition, the 'skin effect' can also be found in the metallic materials. The 'skin effect' was identified in the early works conducted on IN-718 by Pawade *et al* [60], on the nickel-based FGH95 superalloys by Jin *et al* [42, 43], on the D2 tool steels by Kishawy and Elbestawi [61], and on the nickel-based ME16 superalloys by Veldhuis *et al* [62]. Therefore, the 'skin effect' exists not only in the hard and brittle materials, such as ceramics, semiconductor materials, and glasses, but also in the metallic materials, such as superalloys and tool steels.

The 'skin effect' is an intrinsic property that governs the damage behavior of the engineering materials. The 'skin effect' can be interpreted as 'material damage (e.g. cracking, dislocation, phase transformation) is localized if the material is loaded at a high strain rate'. In the case of machining, for example, SSD depth decreases at an increased machining speed (strain rate), and vice versa.

3. Mechanisms of the 'skin-effect' of damage at high strain rates

3.1. Material embrittlement

Generally, a material subjected to machining undergoes plastic deformation before it fractures. The plastic deformation is governed by dislocation motion which is dependent on strain and strain rate. The relationship between the dislocation motion and strain rate is inferred based on the Orowan theory
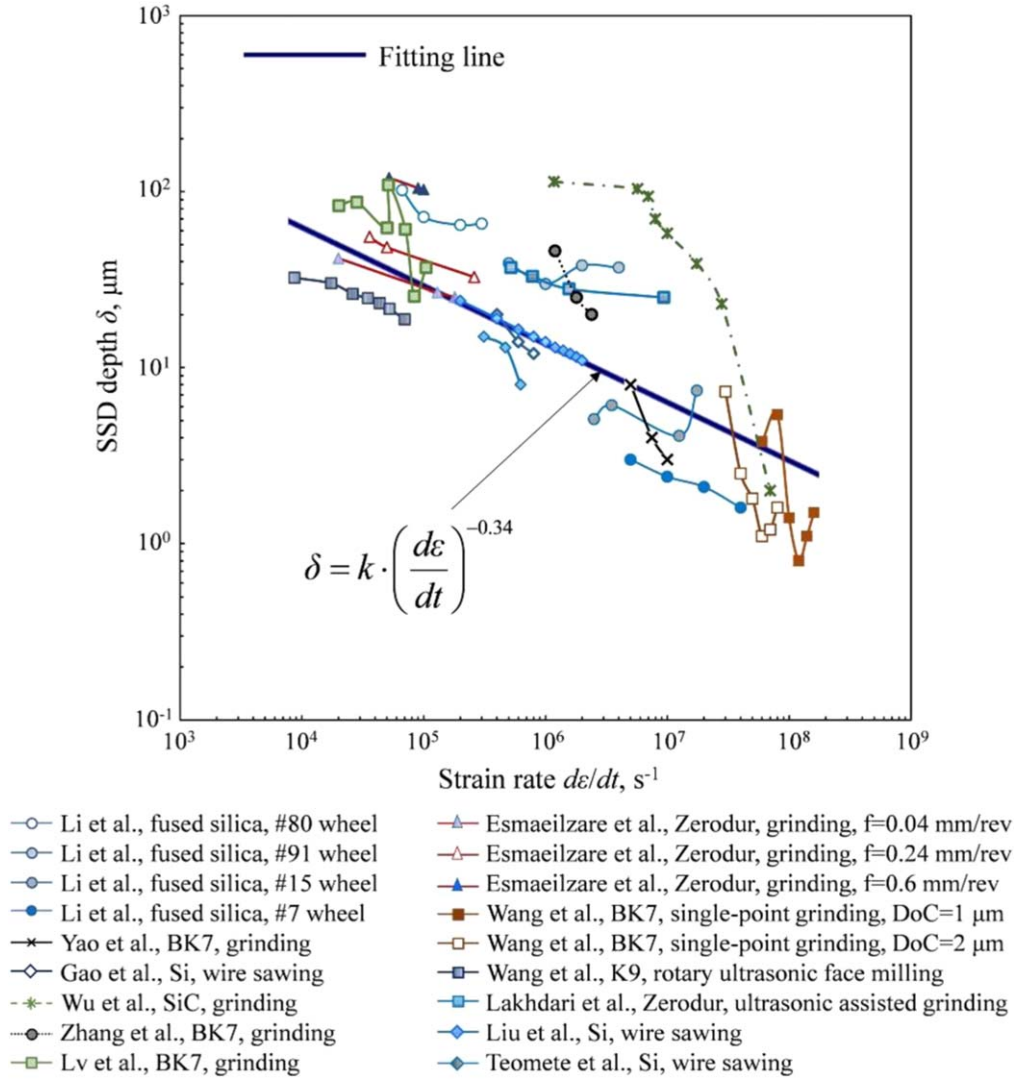
Figure 3. SSD depth of the hard and brittle materials at different strain rates in machining [22, 49–59]. Other conditions are provided in the figure legends.

[63], as given in equation (4),

$$\frac{d\varepsilon}{dt} = \rho b v, \tag{4}$$

where ρ is dislocation density; b is the magnitude of the Burger's vector; and v is dislocation velocity [64, 65]. However, equation (4) only describes an instantaneous motion of a dislocation excluding the dynamic behaviors, such as nucleation, immobilization, recovery, and annihilation. Therefore, a more adequate model is needed. Strain ε can be calculated by equation (5) [66],

$$\varepsilon = \rho b L, \tag{5}$$

where L is the average displacement of a dislocation. Then, the relationship between the dynamic behaviors of dislocations and strain rate can be inferred by differentiating both sides of equation (5),

$$\frac{d\varepsilon}{dt} = \frac{d(\rho b L)}{dt} = \frac{d\rho}{dt}bL + \rho b \frac{dL}{dt}, \tag{6}$$

Therefore, the strain rate in machining is obtained as

$$\frac{d\varepsilon}{dt} = \frac{d\rho}{dt}bL + \rho b v, \tag{7}$$

where $d\rho/dt$ is the change rate of dislocation density. The right side of equation (7) has two terms, the first term representing the nucleation and annihilation of dislocations and the second term representing dislocation movement [67]. The dislocation velocity v can be resolved by the applied shear stress [67]

$$Cv = b\tau, \tag{8}$$

where C is the drag coefficient due to lattice viscosity and τ is the applied shear stress. As shown in figure 4, the dislocation velocity increases with the applied shear stress, but by an upper limit. The dislocation velocity is bounded by the phonon drag effects [67–70] with the time between obstacles [71], the dislocation velocity does not exceed the sound velocity in the material [72, 73]. At a strain rate high enough to the extent that the moving dislocations cannot effectively accommodate
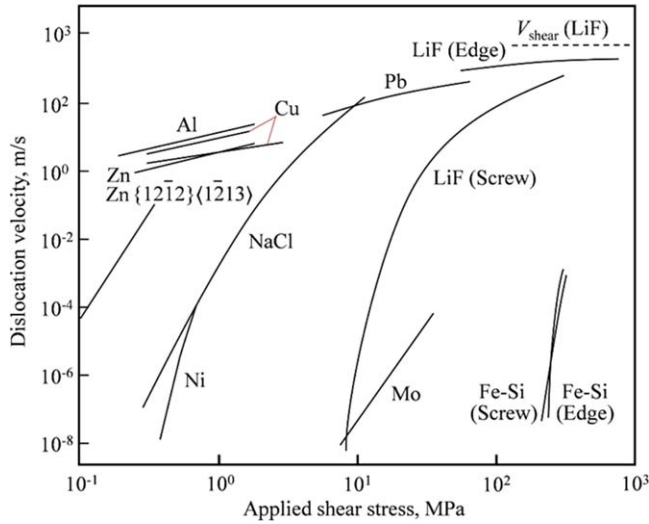
Figure 4. Relationship between dislocation velocity and applied shear stress for different materials. [74] John Wiley & Sons. © 1994 WILEY-VCH Verlag GmbH & Co. KGaA, Weinheim.
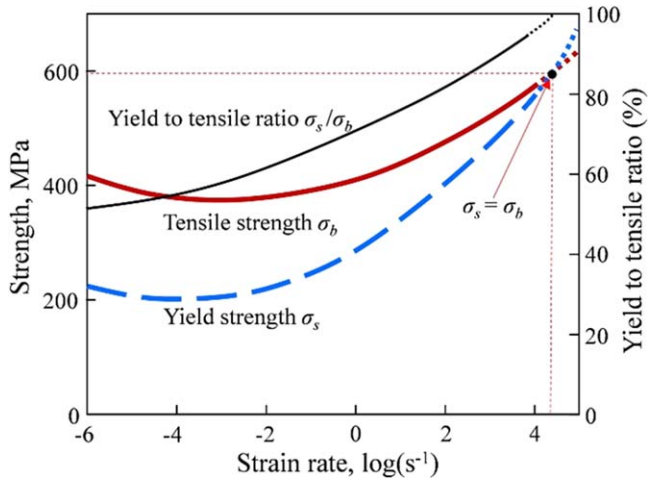
Figure 5. Strain rate dependency of material strengths [77, 78].

loading, more dislocations nucleate, emitting at the sound velocity, and resulting in a dislocation avalanche.

Dislocations can be classified into two types, mobile and immobile. The mobile dislocations may be trapped by each other and turned into immobile ones because of their interactions, including entanglement, attraction, obstruction, etc. Therefore, material deformation enhances not only dislocation nucleation and motion, but also dislocation immobilization. The accumulation of the immobile dislocations increases the resistance to plastic deformation and leads to material hardening [75]. At a high strain rate, dislocation avalanche may dramatically increase the density of the immobile dislocations which are responsible for material hardening. Consequently, the plastic deformation of a material is suppressed before fracturing, namely, the material is embrittled.

In terms of the strength enhancement, both tensile strength σ_b and yield strength σ_s increase with strain rate, as shown in figure 5. However, as strain rate increases, the yield stress increases more rapidly than the tensile strength and the

yield-to-tensile ratio σ_s/σ_b increases. At a high strain rate ($> 10^4\,\mathrm{s}^{-1}$), the yield strength approaches the tensile strength. As a limit, the yield strength can be the same as but never surpass the tensile strength [76]. In this case, the material fractures prior to yielding, which is a typical characteristic of a brittle material. Material embrittlement due to the strain rate effect is thus realized.

As shown in equation (2), strain rate is determined based on cutting speed and depth of cut in the case of machining. Therefore, the strain-rate evoked embrittlement can be acquired by increasing cutting speed and decreasing depth of cut. As shown in figure 6 (a), at a cutting speed of $1000\,\mathrm{m\,min}^{-1}$, the cutting chip exhibited a typical continuous morphology for a ductile material, such as an aluminum alloy. However, as the cutting speed increased to $5000\,\mathrm{m\,min}^{-1}$, the chip morphology turned to be fragmental, as shown in figure 6(b), which means that the material has been embrittled under this condition.

For brittle materials, Lawn and Marshall first proposed that the ratio of hardness to fracture toughness should be used to estimate the brittleness of a material [80]. Boccaccini studied the machinability of a glass-ceramics in terms of the material brittleness represented in equation (9)

$$B = \frac{H}{K_C}, \tag{9}$$

where H and K_c are the hardness and fracture toughness of the material, respectively.

It should be pointed out that material hardness H is strain-rate sensitive and generally increases with strain rate [16, 45, 81–85] due to the strain-rate hardening effect. A correlation between hardness and strain rate is expressed in equation (10) [86]

$$H \propto \left(\frac{d\varepsilon}{dt}\right)^m, \tag{10}$$

where m represents strain-rate exponent, and $m = 0$ for a rigid-perfectly plastic material and $m = 1$ for a linear viscous solid, respectively [87, 88]. Hardness has a power law dependence on strain rate.

The variation in fracture toughness is complicated. Machado *et al* found that the fracture toughness of CFRP decreased as strain rate increased [89, 90]. Anton *et al* found that the dynamic fracture toughness of the Pyrex glass was greater than the static fracture toughness. However, for the magnesia partially-stabilized zirconia and yttria-tetragonal zirconia polycrystals, the dynamic fracture toughness was smaller than the static fracture toughness [91]. Generally, the fracture toughness of a material is larger at a high strain rate than under the static or quasi-static condition. Suresh *et al* found that the ratio of the dynamic to static fracture toughness was in the range of 1.1–1.6 for brittle ceramics [92]. Liu *et al* studied the high-speed grinding of silicon carbide ceramics and concluded that the dynamic fracture toughness was related to strain rate [93]. Even if both the hardness and fracture toughness increase with strain rate, the former demonstrates a higher rate of increase than the latter. Therefore, as the strain rate increases, the brittleness of a material increases accordingly.
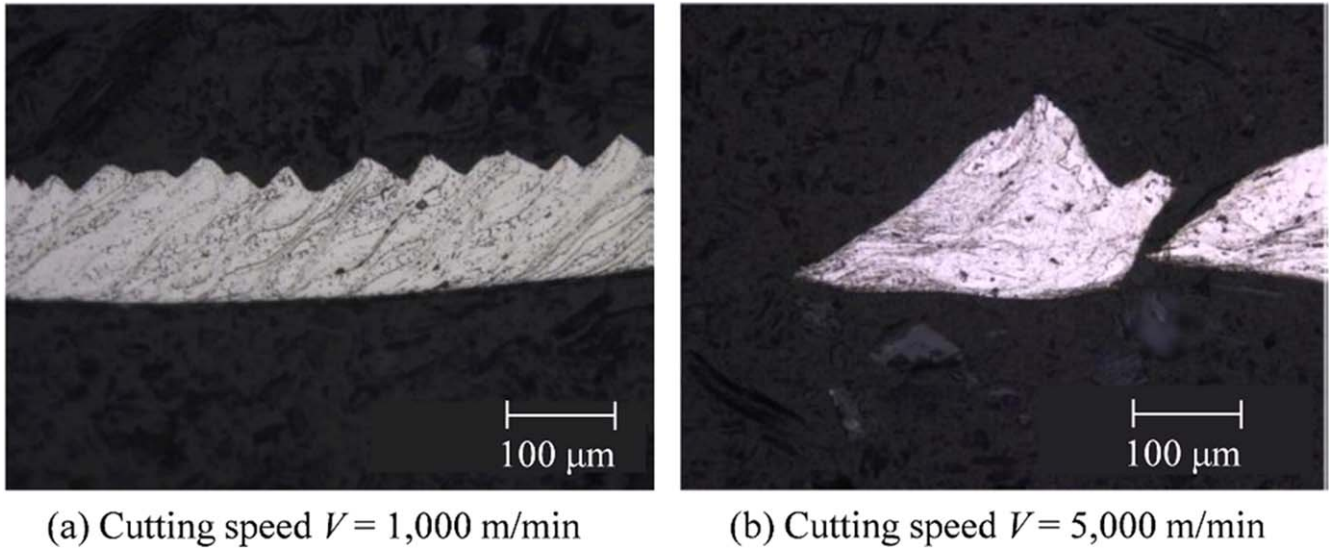
Figure 6. Chip morphologies of 7050-T7451 aluminum alloy with the uncut chip thickness of 0.1 mm and the cutting speeds (a) $V = 1000$ m min^{-1} and (b) $V = 5000$ m min^{-1}, respectively. Reproduced with permission from [79].
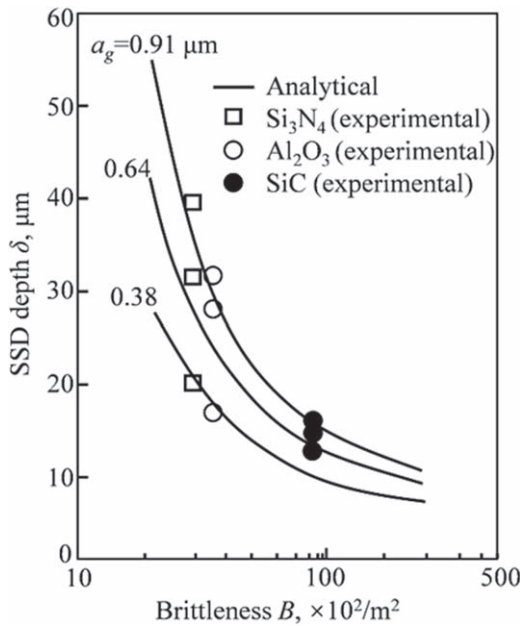
Figure 7. Variation of SSD depth with material brittleness. Reprinted from [94], Copyright (1995), with permission from Elsevier.

Zhang *et al* studied the effect of brittleness of ceramics in grinding on SSD depth and found that the SSD depth decreased as brittleness of ceramics increased [94], which is explained in figure 7. They presented an analytical equation for SSD depth δ in equation (11),

$$\delta = \kappa \cdot a_g^{1/\log(\lambda \cdot B)}, \qquad (11)$$

where κ and λ are constants; a_g is the grit depth of cut. Equation (11) depicts that in grinding of ceramics, SSD depth can be suppressed by increasing brittleness of ceramics, which is obtained with an increased strain rate in high-speed grinding. In other words, the 'skin effect' of SSD distribution exists in machining of materials at an increased speed.

3.2. Dislocation kinetics

Dislocations can be responsible for the formation of grain boundaries and cracks. The movement of dislocations is essential to the evolution of damage. Under an external loading condition, dislocation nucleation, multiplication, and motion are to dissipate the loading energy. The dislocations in a material may be attracted to the free surface by the image force [95–98]. As a result, the dislocation density in the skin layer of the material is higher than that in the deeper layers. In addition, dislocation density should have a larger gradient at a higher strain rate, and vice versa. If the dislocation density is not high enough to accommodate the loading from machining, for example, the dislocation entanglement should first take place in the skin layer, followed by grain refinement and cracking. Therefore, at a high strain rate, the distribution of SSD follows the 'skin effect'.

3.3. Stress wave effect

At high strain rates, the contribution of stress waves to the 'skin effect' of SSD distribution should be taken into consideration. As shown in figure 8, the compressive stress waves are produced due to the high-speed squeezing by a cutting tool. The stress waves propagate along the cutting direction and they are partially reflected by the free surface because of the shortest propagation distance. The compressive stress waves can be converted to tensile stress waves from the free surface reflection, which was also described by Hopkinson [99]. Following this line of reasoning, the reflection waves near the free surface may produce tensile stress that is unbearable for an embrittled material. Consequently, cracks mushroom near the free surface. This may be the reason for the results that the rear portion (with stress wave reflection) were with more damage than the front portion of the sample subjected to impact loading in the study conducted by Jiang *et al* [100]. The impact energy is rapidly dissipated by the mushrooming of the cracks.
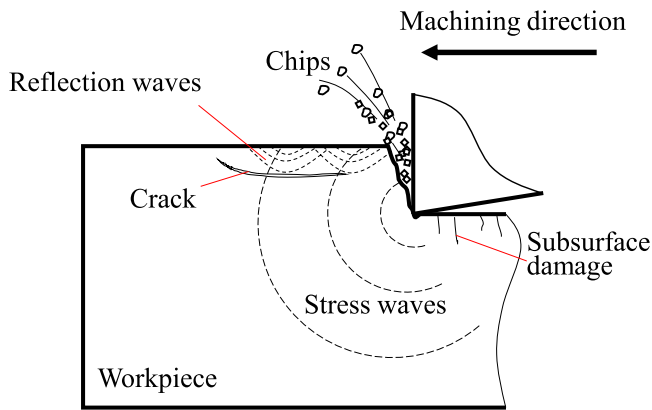
Figure 8. Schematic of stress waves propagating in the workpiece in high-speed machining.

Correspondingly, the cracks are more concentrated in than away from the surface layer of the workpiece.

3.4. Cracking

Generally, SSD is dependent on stress distribution. Based on the Boussinesq elastic-field theory [101], as illustrated in figure 9, there is an elastically stressed (strained) region beneath the loading point. For an indenter with a sharp tip, the stress level approaches infinity around the tip and decreases away from the tip. However, the stress cannot approach infinity since a material should yield or fracture as the stress exceeds the material strength. The region is subjected to hydrodynamic stress and shear stress which may result in grain refinement or pulverization.

Material damage is due to the consequence of loading during which energy is consumed by the material subjected to loading. Damage is dependent not only on the intensity of loading stress but also on the process of loading. In other words, it is also dependent on the strain rate during loading. At an increased strain rate, the damage increases correspondingly [100, 102]. Ping *et al* found that the energy density in breaking a rock increased with the power law of strain rate [103]. At a high strain rate, the number of small cracks rapidly increases to effectively absorb the impact energy, the intersection of the small cracks results in the comminution of a material. Therefore, material fragmentation increases with strain rate, as shown in figure 10.

Grady proposed a model to predict fragment size *d*, based on the balance between the kinetic energy and the newly created surface energy, as shown in equation (12) [104],

$$d = \left(\frac{20^{1/2} K_C}{\rho V_S (d\varepsilon/dt)} \right)^{2/3}, \quad (12)$$

where versus is the sonic velocity. The fragment size decreases at an increased strain rate [105]. The limit to the grain refinement is likely to be amorphization, as reported by Zhao *et al* who discovered that the microstructural change in the monocrystalline silicon under a laser-induced shock loading. The surface layer of the silicon was left with layers of micrometer-sized grains, nanometer-sized grains, amorphous

silicon, and finally the intact monocrystalline silicon [106], sequentially in the depth direction.

Figure 11 shows a schematic diagram of SSD in a brittle material subjected to machining. At the top surface is the amorphous layer below which is the pulverization layer. The pulverized material is squeezed by the cutting edge to the two sides of the groove, forming pile-up. Median and radial cracks form around the pulverization layer. If a radial crack extends to the surface, surface chipping occurs.

Stress gradient may also be responsible for the 'skin effect' of SSD. At an increased strain rate, the stress gradient increases, which may result in a concentrated SSD layer beneath the surface. As described in figure 12(a), at a low strain rate in machining, SSD depth is large and so is the chip size. On the other hand, as the strain rate increases, the stress gradient increases, which results in more concentrated SSD in the skin layer of the material. As shown in figure 12(b), the thicknesses of the respective amorphous and pulverization layers decrease, and so does the chip size. In addition, the stress level decays faster due to a higher stress gradient, which results in a reduced SSD depth.

Based on the above analysis, figure 13 describes the distribution of SSD at different strain rates in machining. The material at the front of the cutting tool is subjected to both the deviatoric and hydrostatic stresses. In such a case, the combination of the two stresses tends to form a pulverization zone described by Zhang *et al* [25]. The pulverization zone consists of microscopic cracks and an amorphous layer (or a grain-refined layer). Macro-cracks initiate and propagate from the boundary of the pulverization layer. The free surface of the workpiece has the least resistance to crack propagation compared to the bulk material down below the surface. Therefore, based on the principle of the minimum material resistance, the cracks tend to propagate towards the free surface, which leads to the damage concentration in the surface layer to cause the 'skin effect'. At an increased strain rate, as schematically shown in figure 13(b), the chip size is decreased and the thicknesses of the pulverization and amorphous layers are reduced accordingly. More chipping is expected in the machined surface because of the material embrittlement at the increased strain rate.

4. Discussion

Based on physics, SSD may be caused by lattice mismatch (e.g. dislocations and stacking faults) and bond rupture of a material. Generally, cracking can be a consequence of dislocations. For example, it may result from the accumulation and entanglement of dislocations. Therefore, at high strain rates, the formation and distribution of dislocations follow the 'skin effect' and so does SSD. Dislocations move towards the free surface under the image force, creating 'skin effect', which leads to the dislocations as well as SSD accumulation near the free surface. On the other hand, high strain rates tend to promote dislocation multiplication, which in turn obstructs material deformation and causes the embrittlement to the material. Based on an early grinding study conducted by Zhang and Howes [94] on ceramic materials, SSD depth
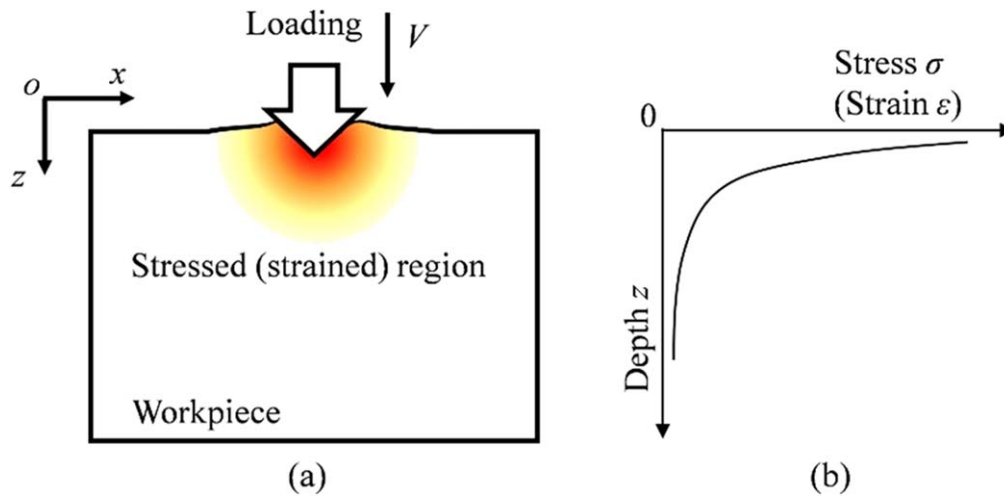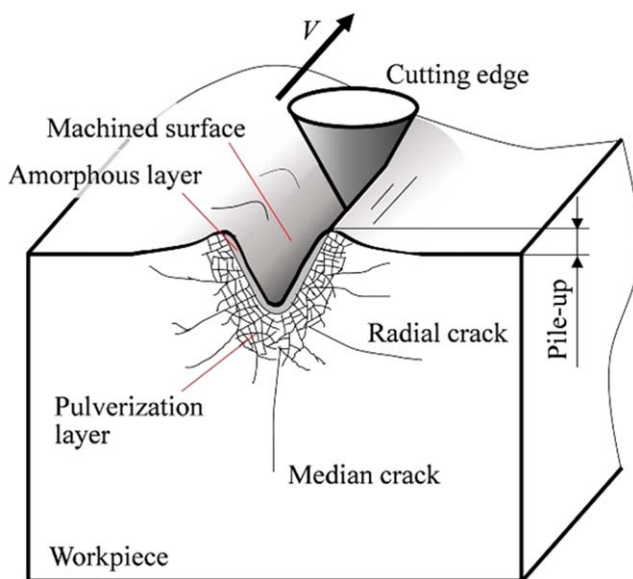
Figure 9. Schematics of (a) a stressed (strained) region around the loading point; (b) stress (strain) distribution in the depth direction.

(a) $\dfrac{d\varepsilon}{dt} = 62.3$ s^{-1} (b) $\dfrac{d\varepsilon}{dt} = 90.2$ s^{-1} (c) $\dfrac{d\varepsilon}{dt} = 114.7$ s^{-1}
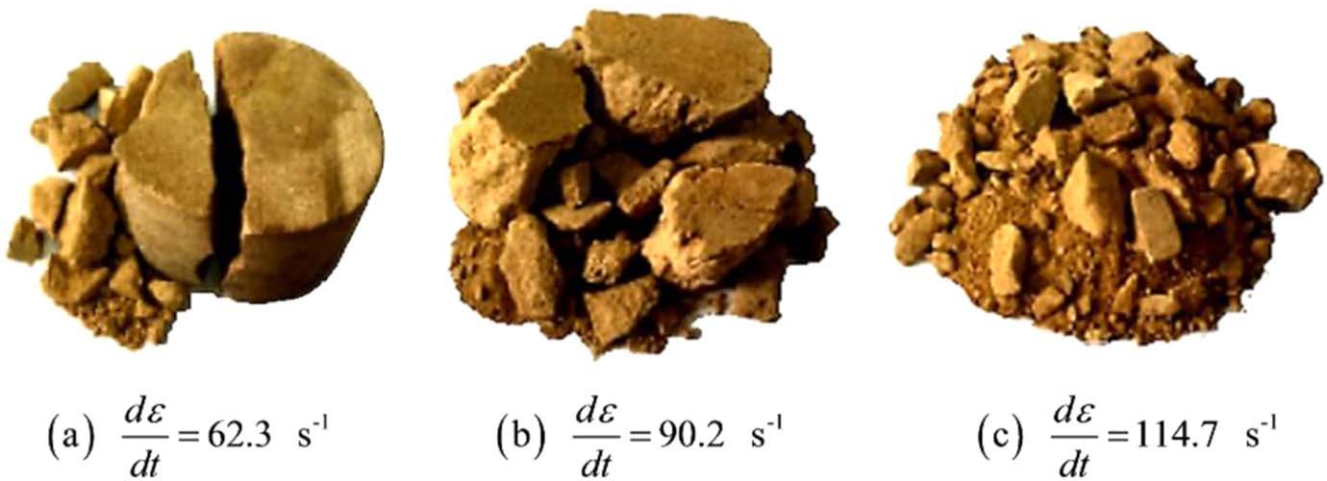
Figure 10. Fragments of sandstone impacted at different strain rates. Reproduced with permission from [102].

Figure 11. Subsurface damage of brittle materials.

decreases with an increase in the material brittleness. Therefore, the 'skin effect' of the dislocations and the material embrittlement due to dislocation multiplication lead to the 'skin effect' of SSD at high strain rates.

Practically, numerous factors, such as strain and strain rate, dislocation movement, crack initiation and propagation, material phase transformation, stress distribution, and stress wave propagation, as well as the changes in the material properties, are collectively responsible for the 'skin effect' of SSD. It is difficult to analyze the 'skin effect' from one factor alone. However, the effect can be comprehended from the aspect of energy dissipation.

From the energy point of view, machining is recognized as an energy rebalance process. A system with the minimum energy level is the most stable. A material in machining is activated with an elevated energy that has a tendency to transform into the most stable state of the minimum energy. The material damage, including dislocations and cracking, is a way of energy relaxation. Based on the minimum energy principle, the damage tends to move towards where the
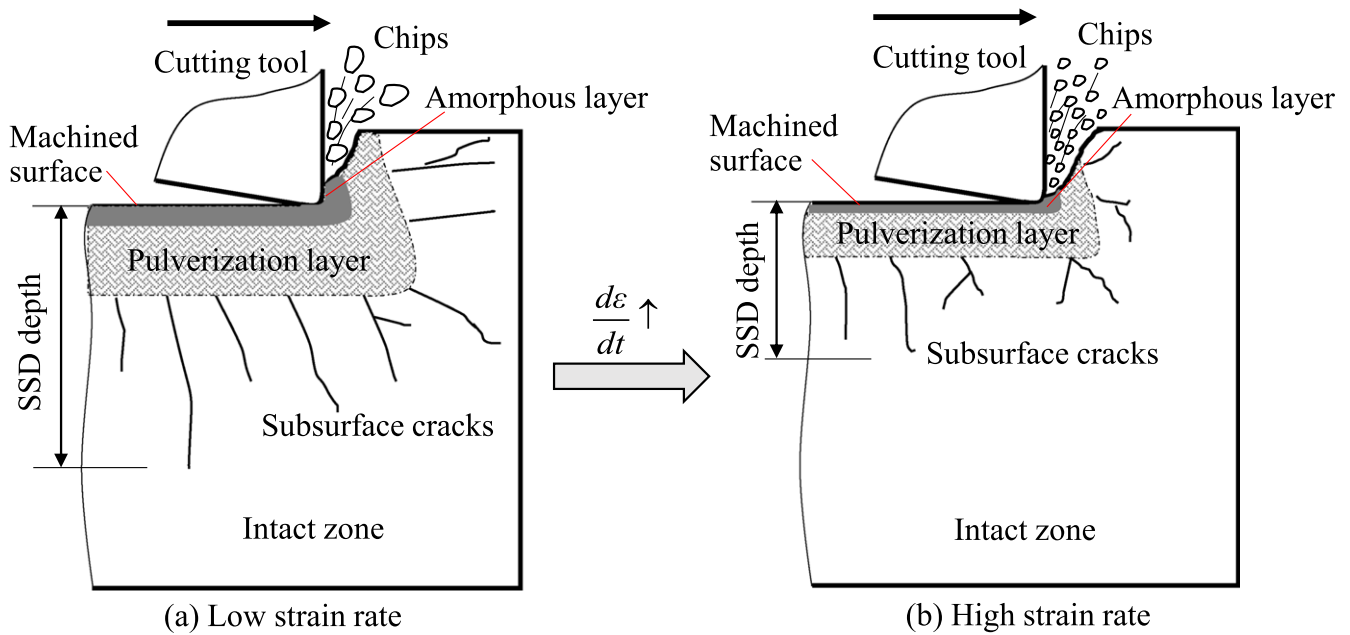
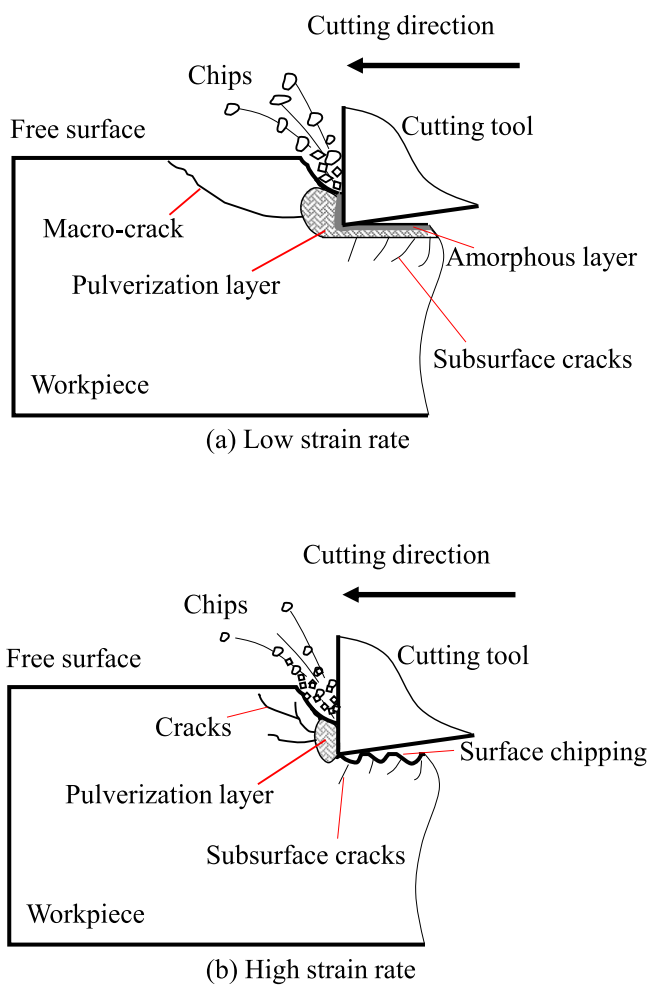**Figure 12.** Subsurface damage evolution with strain rate.

Figure 13. Propagation of macro-cracks at different strain rates.

energy requirement is the lowest for damage formation. Since the free surface has the lowest energy for damage formation compared to other locations within the material, damage tends to propagate towards the free surface.

In this paper, the effect of temperature rise on damage formation in machining is temporarily put aside to simplify the discussion. The temperature in machining indeed affects the mechanical behavior of a material, such as dislocation kinetics [107, 108], stress wave propagation, and eventually surface integrity of a machined part. Specifically, in the conventional machining of ductile materials, temperature has a notable effect on the generation of the surface metamorphic layer [17, 20, 109]. Whereas at the high strain-rate machining, the temperature effect can be neglected. The reason is expatiated in the following.

Temperature rise is a reflection of the heat generation in machining. The heat in machining of a ductile material is mainly generated from material shear and friction. However, at a high strain rate, the material is embrittled, which directly contributes to the heat reduction from the decreased shear and friction and thus to the temperature reduction accordingly.

The 'skin effect' of damage at high strain rates provides a guidance for many industrial applications. In machining, the 'skin effect' allows to acquire the desired surface quality of a machined part by increasing strain rate in machining, such as ultrasonic assisted machining and peening.

5. Concluding remarks and outlook

This paper proposes the 'skin effect' of material damage at high strain rates for the first time. The 'skin effect' is applicable not only to the hard and brittle materials, but also

to most other engineering materials, such as metallic materials. The paper draws the following concluding remarks.

(a) The 'skin effect' of damage is obtained at a high strain rate in a loading process.

(b) High strain rate results in an increase in material brittleness.

(c) Brittleness is a material property that contributes to the 'skin effect' of damage in a loading process;

The 'skin effect' of damage can have numerous industrial applications. One direct application is the HSM of the difficult-to-machine materials, such as ceramics, high strength metals, and composite materials. Nevertheless, many issues remain unresolved, such as how high the stain rate should be in order to suppress SSD in machining. Other issues may include dislocation nucleation and motion, interactions among dislocations during loading at a high strain rate.

With a rapid development of the modern testing equipment and techniques, to have well-controlled testing conditions comes to reality. High-speed and high precision machine tools are readily available. In addition, the state-of-the-art characterization facilities, such as the focused ion beam device in combination with high-resolution transmission electron microscopes (HRTEM), the cathode luminescence device in combination with SEM, are also readily accessible. With the aforementioned modern testing equipment and techniques, the unresolved issues are expected to be resolved, and the underlying physical mechanisms of the 'skin effect' of damage can further be explored in the near future.

Acknowledgments

References

[1] Gao Y 2014 Study on high strian rate deformation of alumina, silicon carbide ceramics and Al_2O_3/SiC nanocomposites *School of Materials Science and Technology* (Beijing: China University of Geosciences)

[2] Sternberg J 1989 Material properties determining the resistance of ceramics to high velocity penetration *J. Appl. Phys.* **65** 3417–24

[3] Ulutan D and Ozel T 2011 Machining induced surface integrity in titanium and nickel alloys: a review *Int. J. Mach. Tools Manuf.* **51** 250–80

[4] Thakur A and Gangopadhyay S 2016 State-of-the-art in surface integrity in machining of nickel-based super alloys *Int. J. Mach. Tools Manuf.* **100** 25–54

[5] Hahn P O 2001 The 300 mm silicon wafer—a cost and technology challenge *Microelectron. Eng.* **56** 3–13

[6] Wang Z, Tian B, Pantouvaki M, Guo W, Absil P, Van Campenhout J, Merckling C and Thourhout D V 2015 Room-temperature InP distributed feedback laser array directly grown on silicon *Nat. Photon.* **9** 837

[7] Pei Z J, Billingsley S R and Miura S 1999 Grinding induced subsurface cracks in silicon wafers *Int. J. Mach. Tools Manuf.* **39** 1103–16

[8] Masuko K *et al* 2014 Achievement of more than 25% conversion efficiency with crystalline silicon heterojunction solar cell *IEEE J. Photovolt.* **4** 1433–5

[9] Taguchi M, Yano A, Tohoda S, Matsuyama K, Nakamura Y, Nishiwaki T, Fujita K and Maruyama E 2014 24.7% record efficiency hit solar cell on thin silicon wafer *IEEE J. Photovolt.* **4** 96–9

[10] Ryu H Y, Jeon K S, Kang M G, Yuh H K, Choi Y H and Lee J S 2017 A comparative study of efficiency droop and internal electric field for InGaN blue lighting-emitting diodes on silicon and sapphire substrates *Sci. Rep.* **7** 44814

[11] Zang Z, Zeng X, Du J, Wang M and Tang X 2016 Femtosecond laser direct writing of microholes on roughened ZnO for output power enhancement of InGaN light-emitting diodes *Opt. Lett.* **41** 3463–6

[12] Lee Y J, Hwang J M, Hsu T C, Hsieh M H, Jou M J, Lee B J, Lu T C, Kuo H C and Wang S C 2006 Enhancing the output power of GaN-based LEDs grown on wet-etched patterned sapphire substrates *IEEE Photonics Technol. Lett.* **18** 1152–4

[13] Yin Z, Huang C, Yuan J, Zou B, Liu H and Zhu H 2015 Cutting performance and life prediction of an Al_2O_3/TiC micro-nano-composite ceramic tool when machining austenitic stainless steel *Ceram. Int.* **41** 7059–65

[14] Shalaby M A, El Hakim M A, Abdelhameed M M, Krzanowski J E, Veldhuis S C and Dosbaeva G K 2014 Wear mechanisms of several cutting tool materials in hard turning of high carbon-chromium tool steel *Tribol. Int.* **70** 148–54

[15] Li H N, Yu T B, Zhu L D and Wang W S 2016 Evaluation of grinding-induced subsurface damage in optical glass BK7 *J. Mater. Process. Technol.* **229** 785–94

[16] Che-Haron C H and Jawaid A 2005 The effect of machining on surface integrity of titanium alloy Ti-6% Al-4% V *J. Mater. Process. Technol.* **166** 188–92

[17] Thakur A, Mohanty A and Gangopadhyay S 2014 Comparative study of surface integrity aspects of Incoloy 825 during machining with uncoated and CVD multilayer coated inserts *Appl. Surf. Sci.* **320** 829–37

[18] Herbert C, Axinte D, Hardy M and Brown P D 2012 Investigation into the characteristics of white layers produced in a nickel-based superalloy from drilling operations *Mach. Sci. Technol.* **16** 40–52

[19] Imran M, Mativenga P, Gholinia A and Withers P 2015 Assessment of surface integrity of Ni superalloy after electrical-discharge, laser and mechanical micro-drilling processes *Int. J. Adv. Manuf. Technol.* **79** 1303–11

[20] Aramcharoen A, Mativenga P T and Manufacturing, L.P. Group 2007 White layer formation and hardening effects in hard turning of H13 tool steel with CrTiAlN and CrTiAlN/ MoST-coated carbide tools *Int. J. Adv. Manuf. Technol.* **36** 650

[21] Zhang B, Shen W, Liu Y, Tang X and Wang Y 1997 Microstructures of surface white layer and internal white adiabatic shear band *Wear* **211** 164–8

[22] Wang C, Fang Q, Chen J, Liu Y and Jin T 2016 Subsurface damage in high-speed grinding of brittle materials considering kinematic characteristics of the grinding process *Int. J. Adv. Manuf. Technol.* **83** 937–48

[23] Yamaguchi H, Srivastava A K, Tan M A, Riveros R E and Hashimoto F 2012 Magnetic abrasive finishing of cutting tools for machining of titanium alloys *CIRP Ann.* **61** 311–4

[24] Zhang B, Tokura H and Yoshikawa M 1988 Study on surface cracking of alumina scratched by single-point diamonds *J. Mater. Sci.* **23** 3214–24

[25] Zhang B and Howes T D 1994 Material-removal mechanisms in grinding ceramics *CIRP Ann.* **43** 305–8

[26] Bifano T G, Dow T A and Scattergood R O 1991 Ductile-regime grinding: a new technology for machining brittle materials *J. Eng. Ind.* **113** 184–9

[27] Zhang B, Zheng X L, Tokura H and Yoshikawa M 2003 Grinding induced damage in ceramics *J. Mater. Process. Technol.* **132** 353–64

[28] Zhang B and Peng X 2000 Grinding damage prediction for ceramics via CDM model *J. Manuf. Sci. Eng.* **122** 51–8

[29] Zhang B 1988 Study on Surface Characteristics of non-oxie ceramics scratched by single point diamond *J. Japan Soc. Precis. Eng.* **54** 587

[30] Zhang B, Tokura H and Yoshikawa M 1988 Study on surface damage of ceramics ground with diamond wheel *J. Japan Soc. Precision. Eng* **54** 1537–43

[31] Liang Z, Wang X, Wu Y, Xie L, Jiao L and Zhao W 2013 Experimental study on brittle–ductile transition in elliptical ultrasonic assisted grinding (EUAG) of monocrystal sapphire using single diamond abrasive grain *Int. J. Mach. Tools Manuf.* **71** 41–51

[32] Zhang J H, Zhao Y, Tian F Q, Zhang S and Guo L S 2015 Kinematics and experimental study on ultrasonic vibration-assisted micro end grinding of silica glass *Int. J. Adv. Manuf. Technol.* **78** 1893–904

[33] Shen J Y, Wang J Q, Jiang B and Xu X P 2015 Study on wear of diamond wheel in ultrasonic vibration-assisted grinding ceramic *Wear* **332-333** 788–93

[34] Gao G F, Zhao B, Xiang D H and Kong Q H 2009 Research on the surface characteristics in ultrasonic grinding nano-zirconia ceramics *J. Mater. Process. Technol.* **209** 32–7

[35] Wang Y, Lin B, Wang S and Cao X 2014 Study on the system matching of ultrasonic vibration assisted grinding for hard and brittle materials processing *Int. J. Mach. Tools Manuf.* **77** 66–73

[36] Wang J, Feng P, Zhang J, Zhang C and Pei Z 2016 Modeling the dependency of edge chipping size on the material properties and cutting force for rotary ultrasonic drilling of brittle materials *Int. J. Mach. Tools Manuf.* **101** 18–27

[37] Cao J, Wu Y, Lu D, Fujimoto M and Nomura M 2014 Material removal behavior in ultrasonic-assisted scratching of SiC ceramics with a single diamond tool *Int. J. Mach. Tools Manuf.* **79** 49–61

[38] Sun Z, To S and Yu K M 2018 An investigation in the ultra-precision fly cutting of freeform surfaces on brittle materials with high machining efficiency and low tool wear *Int. J. Adv. Manuf. Technol.* **101** 1583–93

[39] Shi K, Ren J, Zhang D, Zhai Z and Huang X 2017 Tool wear behaviors and its effect on machinability in dry high-speed milling of magnesium alloy *Int. J. Adv. Manuf. Technol.* **90** 3265–73

[40] Chen J, Fang Q and Li P 2015 Effect of grinding wheel spindle vibration on surface roughness and subsurface damage in brittle material grinding *Int. J. Mach. Tools Manuf.* **91** 12–23

[41] M'Saoubi R, Larsson T, Outeiro J, Guo Y, Suslov S, Saldana C and Chandrasekar S 2012 Surface integrity analysis of machined Inconel 718 over multiple length scales *CIRP Ann.* **61** 99–102

[42] Jin D, Liu Z, Yi W and Su G 2011 Influence of cutting speed on surface integrity for powder metallurgy nickel-based superalloy FGH95 *Int. J. Adv. Manuf. Technol.* **56** 553–9

[43] Du J, Liu Z and Lv S 2014 Deformation-phase transformation coupling mechanism of white layer formation in high speed machining of FGH95 Ni-based superalloy *Appl. Surf. Sci.* **292** 197–203

[44] Yang H C, Chen Z T and Zhou Z T 2015 Influence of cutting speed and tool wear on the surface integrity of the titanium alloy Ti-1023 during milling *Int. J. Adv. Manuf. Technol.* **78** 1113–26

[45] Kaynak Y, Karaca H E and Jawahir I S 2015 Cutting speed dependent microstructure and transformation behavior of NiTi alloy in dry and cryogenic machining *J. Mater. Eng. Perform.* **24** 452–60

[46] Davim J P and Maranhão C 2009 A study of plastic strain and plastic strain rate in machining of steel AISI 1045 using FEM analysis *Mater. Des.* **30** 160–5

[47] Shaw M C 2005 *Metal Cutting Principles–Oxford Series on Advanced Manufacturing* (New York: Oxford University Press)

[48] Wang B, Liu Z, Su G, Song Q and Ai X 2015 Investigations of critical cutting speed and ductile-to-brittle transition mechanism for workpiece material in ultra-high speed machining *Int. J. Mech. Sci.* **104** 44–59

[49] Li Y *et al* 2011 Morphology and distribution of subsurface damage in optical fused silica parts: bound-abrasive grinding *Appl. Surf. Sci.* **257** 2066–73

[50] Esmaeilzare A, Rahimi A and Rezaei S M 2014 Investigation of subsurface damages and surface roughness in grinding process of Zerodur® glass-ceramic *Appl. Surf. Sci.* **313** 67–75

[51] Yao Z, Gu W and Li K 2012 Relationship between surface roughness and subsurface crack depth during grinding of optical glass BK7 *J. Mater. Process. Technol.* **212** 969–76

[52] Wang J, Zhang C, Feng P and Zhang J 2016 A model for prediction of subsurface damage in rotary ultrasonic face milling of optical K9 glass *Int. J. Adv. Manuf. Technol.* **83** 347–55

[53] Gao Y, Ge P and Liu T 2016 Experiment study on electroplated diamond wire saw slicing single-crystal silicon *Mater. Sci. Semicond. Process.* **56** 106–14

[54] Wu C, Li B, Liu Y, Pang J and Liang S Y 2017 Strain rate-sensitive analysis for grinding damage of brittle materials *Int. J. Adv. Manuf. Technol.* **89** 2221–9

[55] Lakhdari F, Bouzid D, Belkhir N and Herold V 2017 Surface and subsurface damage in Zerodur® glass ceramic during ultrasonic assisted grinding *Int. J. Adv. Manuf. Technol.* **90** 1993–2000

[56] Zhang L, Liu W, Chen J and Fang Q 2018 Subsurface damage in grinding of brittle materials considering machining parameters and spindle dynamics *Int. J. Adv. Manuf. Technol.* **97** 3723–34

[57] Lv D, Huang Y, Tang Y and Wang H 2013 Relationship between subsurface damage and surface roughness of glass BK7 in rotary ultrasonic machining and conventional grinding processes *Int. J. Adv. Manuf. Technol.* **67** 613–22

[58] Liu T, Ge P, Bi W and Gao Y 2017 Subsurface crack damage in silicon wafers induced by resin bonded diamond wire sawing *Mater. Sci. Semicond. Process.* **57** 147–56

[59] Teomete E 2013 Wire saw process-induced surface damage characterization *Arab. J. Sci. Eng.* **38** 1209–15

[60] Pawade R S, Joshi S S and Brahmankar P K 2008 Effect of machining parameters and cutting edge geometry on surface integrity of high-speed turned Inconel 718 *Int. J. Mach. Tools Manuf.* **48** 15–28

[61] Kishawy H A and Elbestawi M A 2001 Tool wear and surface integrity during high-speed turning of hardened steel with polycrystalline cubic boron nitride tools *Proc. Inst. Mech. Eng.* B **215** 755–67

[62] Veldhuis S C, Dosbaeva G K, Elfizy A, Fox-Rabinovich G S and Wagg T 2010 Investigations of white layer formation during machining of powder metallurgical Ni-based ME 16 superalloy *J. Mater. Eng. Perform.* **19** 1031–6

[63] Orowan E 1940 Problems of plastic gliding *Proc. Phys. Soc.* **52** 8

[64] Abu Al-Rub R K and Voyiadjis G Z 2006 A physically based gradient plasticity theory *Int. J. Plast.* **22** 654–84

[65] Loveridge-Smith A *et al* 2001 Anomalous elastic response of silicon to uniaxial shock compression on nanosecond time scales *Phys. Rev. Lett.* **86** 2349–52

[66] Hull D and Bacon D J 2001 *Introduction to Dislocations* (Oxford: Butterworth-Heinemann)

[67] Chen L 2015 The role of temperature and microstructure on the dynamic strength of materials *Physics* (London: Imperial College)

[68] Brailsford A D 1972 Anharmonicity contributions to dislocation drag *J. Appl. Phys.* **43** 1380–93

[69] Gorman J A, Wood D S and Vreeland T Jr 1969 Mobility of dislocations in aluminum *J. Appl. Phys.* **40** 833–41

[70] Nadgornyi E 1988 Dislocation dynamics and mechanical properties of crystals *Prog. Mater. Sci.* **31** 1–530

[71] Follansbee P S and Kocks U F 1988 A constitutive description of the deformation of copper based on the use of the mechanical threshold stress as an internal state variable *Acta Metall.* **36** 81–93

[72] Johnston W G and Gilman J J 1959 Dislocation velocities, dislocation densities, and plastic flow in lithium fluoride crystals *J. Appl. Phys.* **30** 129–44

[73] Gurrutxaga-Lerma B, Balint D S, Dini D, Eakins D E and Sutton A P 2014 chapter two-dynamic discrete dislocation plasticity *Advances in Applied Mechanics* ed S P A Bordas (Amsterdam: Elsevier) pp 93–224

[74] Meyers M A 1994 *Dynamic Behavior of Materials* (New York: Wiley)

[75] Taylor G I 1938 Plastic strain in metals *J. Institute Metals* **62** 307–24

[76] Shigley J E and Mischke C R 1989 *Mechanical Engineering Design* 5th edn (New York: McGraw-Hill)

[77] Wang B, Liu Z, Su G and Ai X 2015 Brittle removal mechanism of ductile materials with ultrahigh-speed machining *J. Manuf. Sci. Eng.* **137** 061002

[78] Zhou L, Shimizu J, Muroya A and Eda H 2003 Material removal mechanism beyond plastic wave propagation rate *Precis. Eng.* **27** 109–16

[79] Wang B and Liu Z 2016 Investigations on deformation and fracture behavior of workpiece material during high speed machining of 7050-T7451 aluminum alloy *CIRP J. Manuf. Sci. Technol.* **14** 43–54

[80] Lawn B R and Marshall D B 1979 Hardness, toughness, and brittleness: an indentation analysis *J. Am. Ceram. Soc.* **62** 347–50

[81] Zhao S, Wang H, Gu J, Guo N, Shao L, Zhang Y, Yao K and Chen N 2018 High strain rate sensitivity of hardness in Ti–Zr–Hf–Be–(Cu/Ni) high entropy bulk metallic glasses *J. Alloys Compd.* **742** 312–7

[82] Wang Q, Liu Z, Wang B, Song Q and Wan Y 2016 Evolutions of grain size and micro-hardness during chip formation and machined surface generation for Ti-6Al-4V in high-speed machining *Int. J. Adv. Manuf. Technol.* **82** 1725–36

[83] dos Santos T, Rossi R, Maghous S and Rosa P A R 2018 Experimental procedure and simplified modeling for the high strain-rate and transient hardness evolution of aluminum AA1050 *Mech. Mater.* **122** 42–57

[84] Shen J, Kondoh K, Jones T L, Mathaudhu S N, Kecskes L J and Wei Q 2016 Effect of strain rate on the mechanical properties of magnesium alloy AMX602 *Mater. Sci. Eng.* A **649** 338–48

[85] Sun J and Guo Y B 2009 A comprehensive experimental study on surface integrity by end milling Ti–6Al–4V *J. Mater. Process. Technol.* **209** 4036–42

[86] Limbach R, Rodrigues B P and Wondraczek L 2014 Strain-rate sensitivity of glasses *J. Non-Cryst. Solids* **404** 124–34

[87] Bower A F, Fleck N A, Needleman A, Ogbonna N and Enderby J E 1993 Indentation of a power law creeping solid *Proc. R. Soc.* A **441** 97–124

[88] Goodall R and Clyne T W 2006 A critical appraisal of the extraction of creep parameters from nanoindentation data obtained at room temperature *Acta Mater.* **54** 5489–99

[89] Machado J J M, Marques E A S, Campilho R D S G and da Silva L F M 2017 Mode II fracture toughness of CFRP as a function of temperature and strain rate *Composites* B **114** 311–8

[90] Machado J, Marques E, Campilho R and da Silva L F 2017 Mode I fracture toughness of CFRP as a function of temperature and strain rate *J. Compos. Mater.* **51** 3315–26

[91] Anton R J and Subhash G 2000 Dynamic Vickers indentation of brittle materials *Wear* **239** 27–35

[92] Suresh S, Nakamura T, Yeshurun Y, Yang K H and Duffy J 1990 Tensile fracture toughness of ceramic materials: effects of dynamic loading and elevated temperatures *J. Am. Ceram. Soc.* **73** 2457–66

[93] Liu Y, Li B, Wu C and Zheng Y 2016 Simulation-based evaluation of surface micro-cracks and fracture toughness in high-speed grinding of silicon carbide ceramics *Int. J. Adv. Manuf. Technol.* **86** 799–808

[94] Zhang B and Howes T D 1995 Subsurface evaluation of ground ceramics *CIRP Ann.* **44** 263–6

[95] Weinberger C R and Cai W 2007 Computing image stress in an elastic cylinder *J. Mech. Phys. Solids* **55** 2027–54

[96] Wang Z J *et al* 2015 Cyclic deformation leads to defect healing and strengthening of small-volume metal crystals *Proc. Natl Acad. Sci.* **112** 13502–7

[97] Eshelby J D and Mott N F 1951 The force on an elastic singularity, philosophical transactions of the royal society of london *Math. Phys. Sci.* A **244** 87–112

[98] Head A K 1953 X. The Interaction of dislocations and boundaries *London, Edinburgh, Dublin Phil. Mag. J. Sci.* **44** 92–4

[99] Hopkinson B 1921 *The Pressure of a Blow* (Cambridge: Cambridge University Press)

[100] Jiang F, Li Z, Wang N, Guo H and Xu X 2016 Research on dynamic characteristics of Shanxi black granite under high strain rates *J. Vib. Shock* **35** 177–82

[101] Boussinesq J 1970 Application des Potentiels l'Etude de l'Equilibre et du Mouvement des Solides Elastiques' (Gauthier-Villars, Paris, 1885) ed S P Timoshenko and J N Goodier *Theory of Elasticity* (New York: McGraw-Hill) pp 398–402

[102] Deng Y, Chen M, Jin Y and Zou D 2016 Investigation of the dynamic characteristics and energy consumption for breaking rocks using the impact load *Pet. Drill. Tech.* **44** 27–32

[103] Ping Q, Luo X, Ma Q and Yuan P 2015 Broken energy dissipation characteristics of sandstone specimens under impact loads *Chin. J. Rock Mech. Eng.* **34** 4197–203

[104] Grady D E 1982 Local inertial effects in dynamic fragmentation *J. Appl. Phys.* **53** 322–5

[105] Lankford J and Blanchard C R 1991 Fragmentation of brittle materials at high rates of loading *J. Mater. Sci.* **26** 3067–72

[106] Zhao S, Hahn E N, Kad B, Remington B A, Wehrenberg C E, Bringa E M and Meyers M A 2016 Amorphization and nanocrystallization of silicon under shock compression *Acta Mater.* **103** 519–33

[107] Chen L Y, He M R, Shin J, Richter G and Gianola D S 2015 Measuring surface dislocation nucleation in defect-scarce nanostructures *Nat. Mater.* **14** 707

[108] Zhu T, Li J, Samanta A, Leach A and Gall K 2008 Temperature and strain-rate dependence of surface dislocation nucleation *Phys. Rev. Lett.* **100** 025502

[109] Herbert C R J, Kwong J, Kong M C, Axinte D A, Hardy M C and Withers P J 2012 An evaluation of the evolution of workpiece surface integrity in hole making operations for a nickel-based superalloy *J. Mater. Process. Technol.* **212** 1723–30